The Frequency-Hopped Cartesian Feedback Linear Transmitter

Majid Boloorian, *Associate Member, IEEE,* and Joseph P. McGeehan

***Abstract*—A frequency-hopped version of the Cartesian feedback linear transmitter for use in future mobile communication systems is introduced. The essential requirements for the successful operation of such a transmitter are discussed. Using the results obtained from a hardware prototype, the problems generated by a hopping carrier are outlined and solutions introduced.**

I. Introduction

THE GROWING demand for mobile communication services in the past two decades and the limited amount of available frequency spectrum have motivated the search for more spectrally efficient communication techniques. In this respect, both frequency hopping (FH) spread spectrum [1] and the use of linear modulation methods [2], [3] offer very attractive options. It therefore seems logical to consider using linear modulation techniques in conjunction with frequency hopping to develop highly spectral efficient communication techniques for use in third generation wireless systems.

The very first requirement for a frequency-hopped linear system is a linear transmitter with a wide enough operating bandwidth to accommodate the range of hopping carrier frequencies. The effectiveness of the Cartesian feedback technique [4]–[7] in linearizing RF amplifiers for the transmission of narrowband signals suggests the possibility of its use in such a system.

When studying the hopping transmitter, there is a need to closely examine issues such as its transient response at both baseband and RF, variations in the RF amplifier nonlinear characteristics with frequency, readjustment of the loop parameters when hopping, and the control signals required for this readjustment.

Perhaps the most important issue is that of control. Fig. 1 shows a block diagram of the frequency-hopped transmitter, indicating the role of digital signal processing (DSP) in controlling the actions of modules such as the voltage-controlled phase-shifter and frequency synthesizer, and in pre-distorting the transmitter input signal. As will be discussed later, the role of digital signal processing in the operation of the frequency-hopped transmitter is very important and extends further than indicated in Fig. 1.

The transmitter RF components must be of a wideband nature in order to accommodate the wide range of carrier frequencies used with the hopping system. This imposes no problem on the transmitter design as sufficiently wideband mixers, power splitter/combiners, etc., are readily available. Thus apart from the need for wideband components, more complex control signals and a frequency-hopped synthesizer, the FH transmitter would be essentially the same as the basic fixed-carrier version.

The question that remains is whether a transmitter built with wideband modules and controlled by a DSP is capable of operating in a frequency-hopped environment. In the following sections, the behavior and limitations of such a transmitter are investigated and solutions proposed.

Manuscript received September 20, 1994; revised November 22, 1995. This work was supported by the Science and Engineering Research Council and GEC Marconi Communications.

The authors are with the Centre for Communications Research, University of Bristol, Bristol, BS8 1TR, U.K.

Publisher Item Identifier S 0018-9545(96)08195-9.

II. Basic Transmitter Operation

The basic fixed-carrier Cartesian transmitter operates by continuously pre-distorting the amplifier input signal to generate the required output [7]. Representing the amplifier transfer characteristics by a complex function $f(x)$, a desired output signal y may be obtained if a predistorted signal x, given by (1), is applied to the amplifier input

$$x = f^{-1}(y). \tag{1}$$

The idea of predistortion can be better understood by considering the simplified transmitter baseband equivalent model in Fig. 2. The linear forward and feedback gains are represented by M and β, and the transmitter input signal given by $ke^{j\phi}$. The RF amplifier output signal is determined by (2). Note that $\varepsilon e^{j\theta}$ is the amplifier input signal and α, $\Phi(\varepsilon)$, and $\rho(\varepsilon)$ represent its linear gain, AM–PM and AM–AM distortions, respectively

$$y = [\alpha\varepsilon + \rho(\varepsilon)]e^{j[\theta+\Phi(\varepsilon)]}. \tag{2}$$

For a large loop gain,[1] i.e., $M\alpha\beta \gg 1$, the magnitude and phase of the predistorted signal are given by (3) and (4), respectively. The large gain results in an output signal which is a linearly amplified version of the transmitter input signal. The linear relationship between the input and output signal is given by (5). In practice, the loop time delay limits the size of the loop gain, and low-pass filters will be required if large loop gains are to be produced. The use of low-pass filters, however, results in lower values of loop gain at high frequencies, leading to smaller transmitter linearization bandwidths (i.e., higher-order intermodulation distortion products will be attenuated less than those of lower orders)

$$\varepsilon = \frac{k}{\alpha\beta} - \frac{\rho(\varepsilon)}{\alpha} \tag{3}$$

[1] Unless specified, the terms loop gain, bandwidth, and delay refer to the open-loop gain, bandwidth, and delay, respectively.

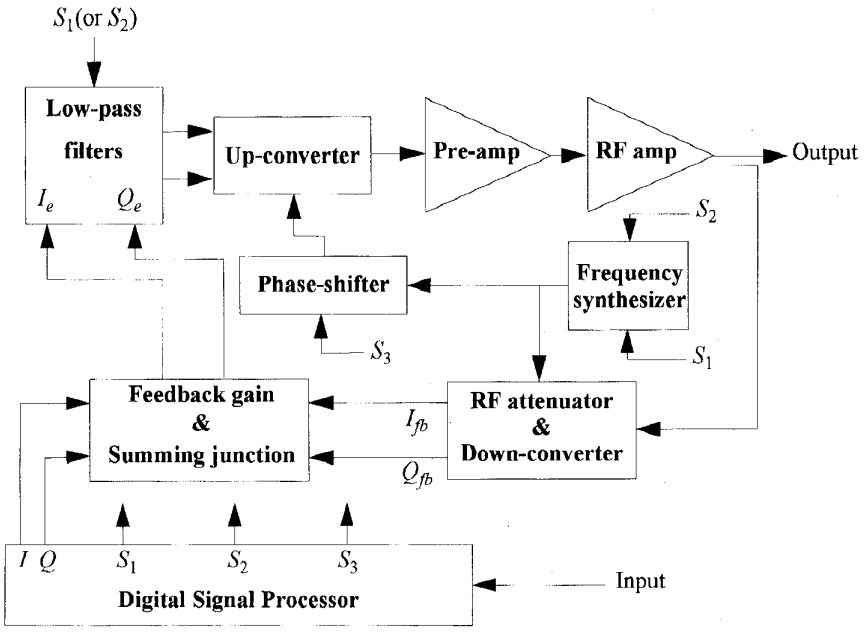

Fig. 1. The block diagram of the frequency-hopped Cartesian transmitter.

$$\theta = \phi - \Phi(\varepsilon) \tag{4}$$

$$y = \frac{1}{\beta}(ke^{j\phi}). \tag{5}$$

The nonlinear nature of the transmitter makes an accurate algebraic study of its performance difficult. Numerical techniques, however, offer more reliable routes, so a simulated model of the transmitter was devised to investigate its properties. This model was validated by comparison with the results from a fully developed transmitter [5]. Fig. 4 shows the input and output signals of the simulated amplifier when the transmitter model was excited by a two-tone signal. The nonlinear characteristics of the amplifier are depicted in Fig. 3. These plots clearly verify the above analysis, and illustrate that in order to obtain the desired output signal, the amplifier input signal needs considerable pre-distortion. The predistortion mechanism becomes clear when the amplifier input signal and nonlinear characteristics are considered together. The envelope of the amplifier input signal is changed so that it counteracts the AM–AM nonlinearities, and the signal phase is modified in the opposite direction to that of the AM–PM characteristic. The net result of these two simultaneous actions is to remove the effect of the nonlinearities from the final output signal. It should be noted that Fig. 4 shows the modulation signals appearing at the input and output of the RF amplifier, and not the RF signals. This is perfectly justified since the Cartesian transmitter is a modulation feedback system and its properties are independent of the carrier signal frequency.

The predistorting action of the transmitter can also be seen by considering the spectrum of the amplifier input signal as shown in Fig. 5. The open- and closed-loop spectra of the transmitter output signal are depicted in Fig. 6 which shows close agreement with the results obtained from the hardware prototype [5]: IMD3 (the third-order intermodulation distortion product) suppression of 51 dB compared to 45 dB for a two-tone separation of 5 kHz.

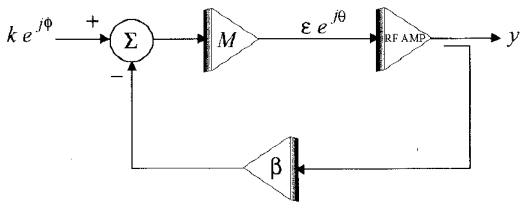

Fig. 2. Simplified loop diagram.

The success of the feedback method depends on the level of pre-distortion it can generate, which in turn is dependent upon the value of the loop gain which can be tolerated before instability is reached [7]. The AM–AM and AM–PM characteristics of the simulated 5 kHz linear transmitter are shown in Fig. 7. It can be seen that the transmitter AM–AM characteristic is virtually a linear function of its input signal level, and its AM–PM characteristic is almost flat, fluctuating by only 0.8° about a fixed value (this should be compared with the 55° variation of the amplifier AM–PM characteristic).

A. Transmitter Stability

When designing the transmitter, a knowledge of its stability limits, which determine its successful operation, is essential. The condition for the stability of a linear first-order feedback loop is given by (6) (see Appendix A) where G, BW, and D represent loop gain, 3-dB bandwidth (in Hz), and delay (in seconds), respectively. The results of a large number of simulations have revealed that a similar condition exists for the stability of the Cartesian transmitter: its stability is maintained as long as the value of its gain-bandwidth-delay (*GBWD*) product does not exceed a constant. The value of this constant

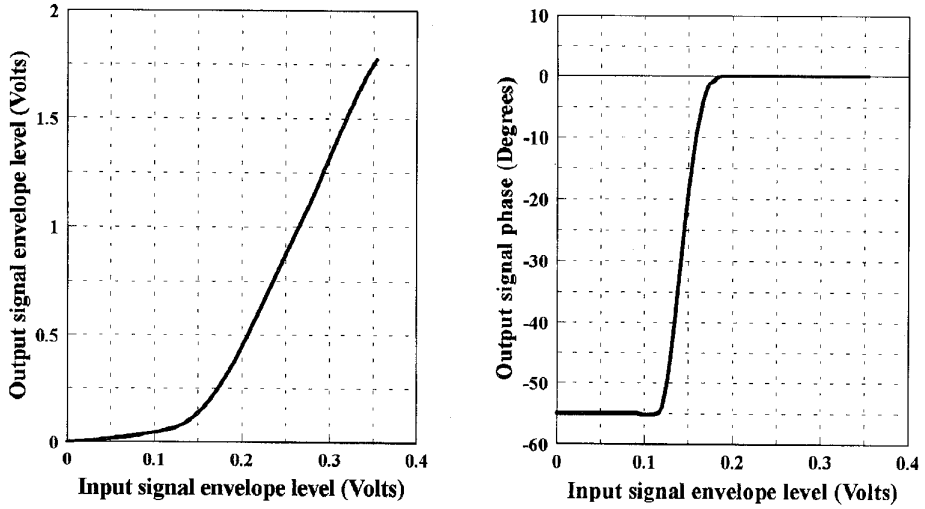

(a) (b)

Fig. 3. AM–AM and AM–PM characteristics of the amplifier used in simulation.

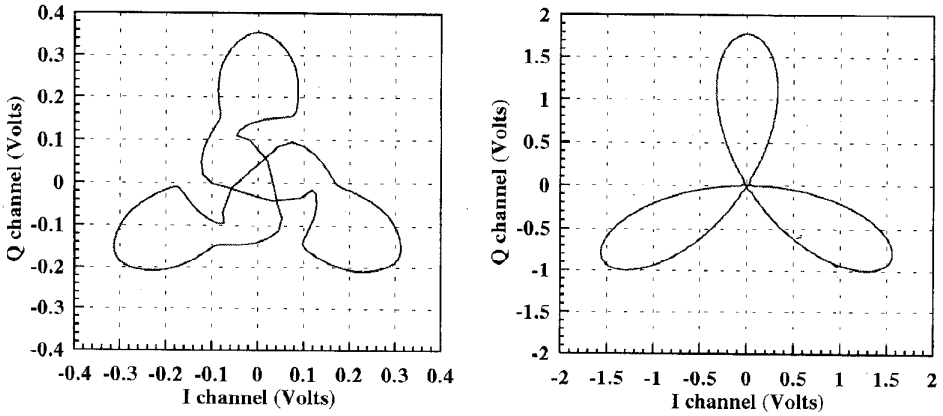

(a) (b)

Fig. 4. Simulation results: amplifier input and output modulation signals on the complex plane.

is determined by the characteristics of the transmitter nonlinear components (mainly the amplifier)

$$GBWD < 0.25. \tag{6}$$

The gain component of the $GBWD$ product is the total gain of the loop linear components and does not include the nonlinear gain generated by the RF amplifier. Since the linear components determine the adjustable part of the loop gain, the exclusion of the amplifier gain from $GBWD$ is justifiable. It should be kept in mind, however, that the actual value of the loop gain includes a component generated by the amplifier.

B. Transmitter Baseband Transient Response

In applications such as TDMA and frequency hopping where the transmitter input signal can be turned on and off frequently, the speed of the transmitter in responding to the rapid changes in its input signal level, i.e., its baseband transient response, becomes an important issue.

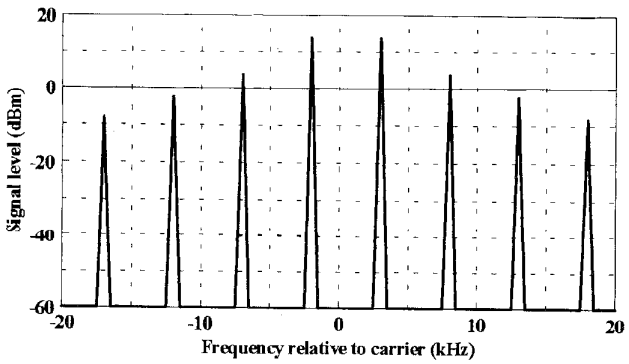

Fig. 5. Simulation results: spectrum of the predistorted signal.

The effects of loop time delay on the transient response of a first-order linear system are discussed in Appendix D. It is shown that the loop delay makes a first-order loop behave like a higher-order system. When the first-order system with time delay is approximated by a second-order system, its

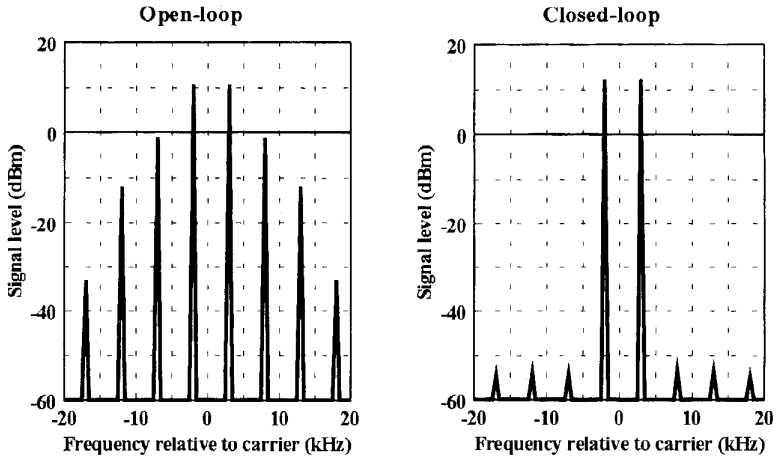

Fig. 6. Simulation results: open- and closed-loop performance of the transmitter.

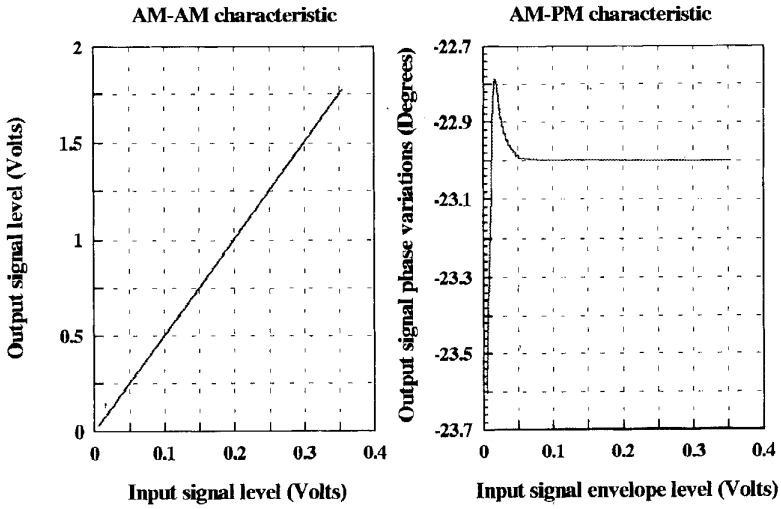

Fig. 7. Simulation results: AM–AM and AM–PM characteristics of the closed-loop transmitter.

transient response is shown to be determined by the size of its $GBWD$ product. The transient response of such a loop exhibits overshoots when the value of $GBWD$ product is high.

The simulation results show that the transient response of a first-order Cartesian transmitter is also determined by the size of its $GBWD$ product. Fig. 8 illustrates the transient response of the simulated transmitter for the cases with high and low values of $GBWD$ product. It is seen that in the case of high $GBWD$ product, the transient response exhibits overshoots when the transmitter input signal level is high. No overshoots are observed when the input signal level is low or on the falling edges of the output waveform.

This behavior can be explained by considering the AM–AM characteristic of the amplifier. At high levels of transmitter input signal, the amplifier gain is high, which results in a large instantaneous value of loop gain. The presence of loop delay becomes significant at high values of loop gain and the transmitter behaves like a higher order system, thus overshoots appear on the rising edges of the output waveform. When the input signal level is low, the amplifier gain is low and the system behaves more like an ideal first-order system, and therefore no overshoots are observed. As seen in Fig. 8, the variations of the transient response with the input signal level may be minimized by reducing the value of the $GBWD$ product. However, improvement in the transient response will be at the expense of lower attenuation of the IMD products. Alternatively, the transmitter input signal can be shaped to achieve better transient response. In practice, it may be necessary to use a combination of the two techniques to improve the baseband transient response of the transmitter.

C. Main Loop Parameters

Although the Cartesian transmitter is a nonlinear feedback system, it is possible to predict its general properties by considering linear feedback loops. For this reason, the analysis of the performance of a linear feedback system is included in the appendices to assist a better understanding of the transmitter behavior. As in the first-order linear systems, the main parameters which govern the Cartesian transmitter performance are: its loop gain, 3-dB bandwidth and time delay.

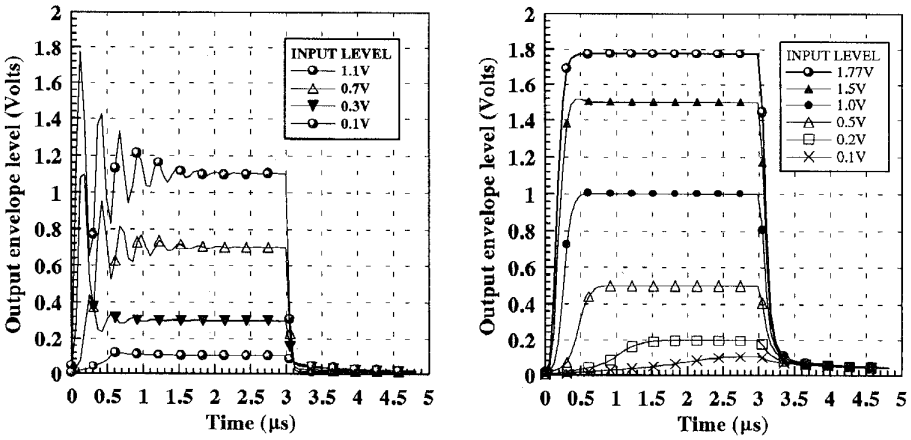

Fig. 8. Baseband transient response of the simulated transmitter with (a) high and (b) low $GBWD$ products.

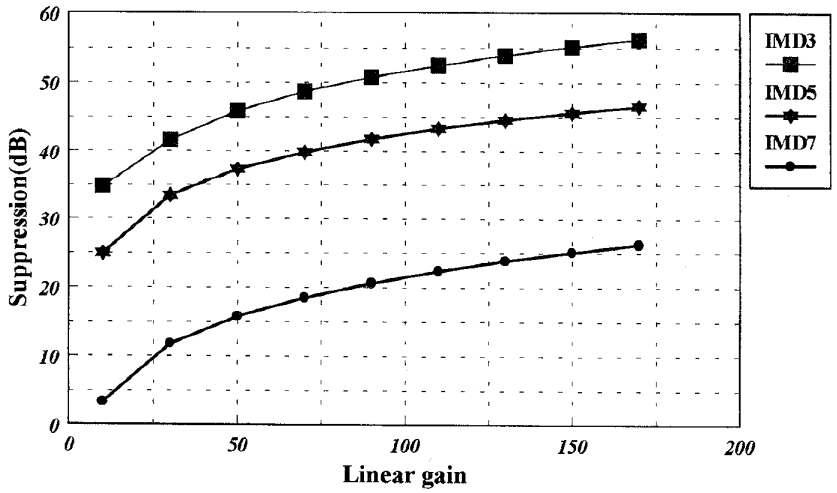

Fig. 9. Simulation results: variations of IMD products suppression with loop linear gain (fixed BWD product).

In this section, the effects of each of these parameters on the performance of the simulated transmitter are discussed and the similarities between the transmitter operation and that of the linear first-order systems are highlighted.

1) Loop Gain: The effect of a forward path unwanted signal (a disturbance) on the output of a first-order linear system can be minimized by maximizing the value of loop gain (39). A similar argument applies to the first-order Cartesian transmitter: as long as the loop stability limits are not exceeded, the attenuation levels of the various IMD products (viewed as disturbance) can be increased by increasing the value of loop linear gain.

Fig. 9 shows the plot of the suppression levels of the simulated transmitter IMD products versus loop linear gain. It can be seen that the suppression levels improve asymptotically with an increase in the loop linear gain. The suppression level is higher for lower-order IMD products. This of course is due to higher loop gain nearer to the carrier, resulting from the low-pass filters' operation. The asymptotic nature of these plots may be predicted by considering the disturbance attenuation at the output of a linear first-order system given by (40).

2) Loop 3-dB Bandwidth: Equation (40) also indicates that for a given value of loop gain, the attenuation levels of higher-order IMD products may be increased by increasing the loop 3-dB bandwidth. The suppression level of the IMD products whose frequency is less than the loop filter 3-dB frequency is not significantly affected by this increase. However, considering the upper limit of $GBWD$ product for a stable loop, an increase in the size of the filter 3-dB bandwidth will limit any further increase in the loop linear gain, which in turn limits the distortion-removing capability of the transmitter at frequencies nearer to the carrier.

In general, as discussed in Appendix B, for fixed values of $GBWD$ product and loop delay, the performance of a first-order linear system can be enhanced over a large range of frequencies, $\omega \ll A\beta\omega_n$, if the loop gain is increased and the corresponding value of its bandwidth decreased. The same argument may be applied to the Cartesian transmitter: higher degrees of linearity may be achieved by increasing the loop gain and reducing its 3-dB bandwidth while keeping the $GBWD$ product constant (Fig. 10). Thus an integrator used as the loop filter can provide the highest level of linearity for

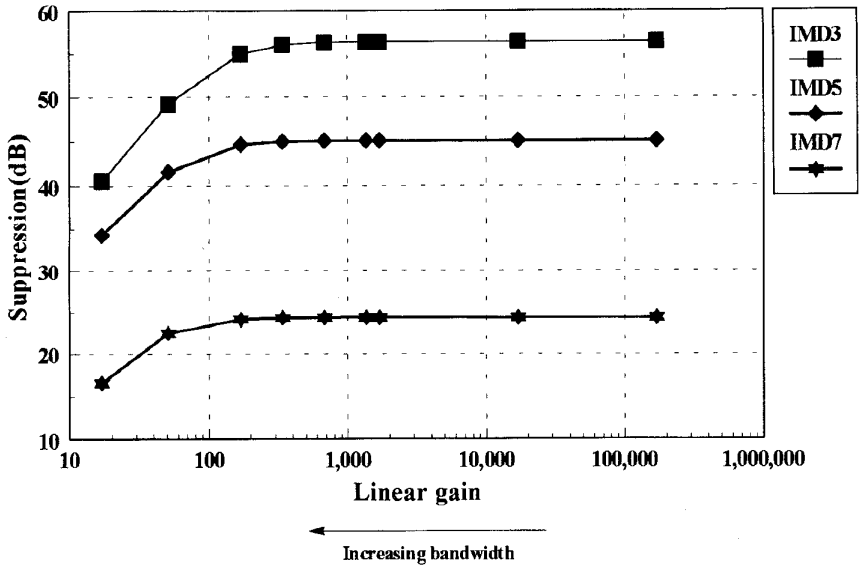

Fig. 10. Simulation results: suppression of IMD products versus loop gain for a fixed GBW product ($GBWD = 0.031$, Delay = 61 ns).

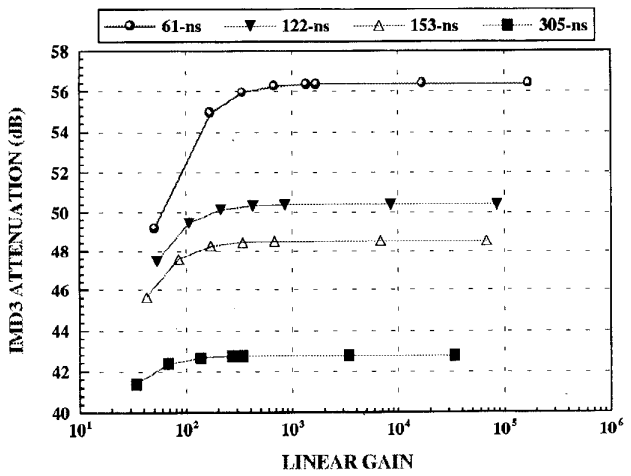

Fig. 11. Simulation results: effect of time delay on transmitter performance.

a given amplifier, generating the largest attenuation of forward loop dc offsets and up-converter mixers' carrier feed-through. The main disadvantage of using an integrator is the very high loop gain applied to any feedback path dc offset resulting in the corruption of the transmitter output signal.

As could be predicted from (41) and Fig. 28 and as can be seen in Fig. 10, the suppression levels of the IMD products vary asymptotically with the loop gain and their improvement rate reduces at higher values of loop gain. Thus, it seems possible to achieve a near optimum performance without having to use an integrator. This is shown to be the case in Fig. 10, where the suppression levels of various IMD products of the simulated transmitter are plotted against the loop linear gain (compare these plots with those in Fig. 28). It can be seen from these plots that in the system under investigation, a near optimum performance is achieved with the loop gain at about 200 and the loop 3-dB bandwidth at approximately 2550 Hz. Beyond this value of loop gain, the improvement is negligible.

3) Loop Delay: As in linear feedback systems, time delay plays a very important part in the performance of the Cartesian transmitter. It results in the bandlimited behavior of the transmitter and makes its stability conditional. The latter imposes an upper limit on the maximum value of the loop gain-bandwidth, GBW, product which in turn limits the distortion-removing capability of the transmitter.

As discussed before, transmitter stability is determined by the maximum value of its $GBWD$ product. An increase in the time delay results in a smaller value for the maximum GBW product, which in turn degrades the linearizing properties of the feedback system. The plots in Fig. 11 show the variations of the attenuation of the simulated transmitter IMD3 with the loop linear gain for a range of values of loop delay with the $GBWD$ product at its maximum. These plots clearly demonstrate that transmitter performance improves significantly with a decrease in loop time delay. It is therefore important to keep the delay as low as possible by using appropriate components and layout at the design stage.

D. Transmitter Linearization Bandwidth

As mentioned in the previous sections, the presence of loop time delay and low-pass filters results in the bandlimited nature of the transmitter performance. The closed-loop 3-dB bandwidth of the transmitter which may be approximated by (45) does not relate to the true frequency range within which the amplifier is successfully linearized. The transmitter linearization bandwidth is determined by the required suppression levels of the IMD products and is defined as the maximum bandwidth within which the required IMD attenuation is achieved.

The linearization bandwidth of a Cartesian transmitter is normally much smaller than its closed-loop 3-dB bandwidth and can be much larger than its open-loop 3-dB bandwidth. In the case of the amplifier under consideration, a 5-kHz linearization bandwidth can be achieved if a 56-dB suppression

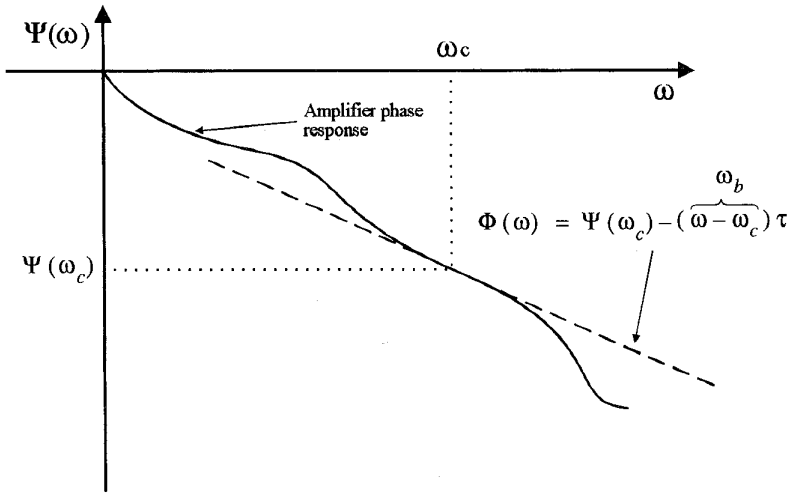

Fig. 12. Linear approximation to RF amplifier phase response.

of IMD3 is required (delay = 61 ns). Larger linearization bandwidths are possible if smaller suppression of IMD3 is acceptable. The closed-loop bandwidth of the transmitter is about 10 MHz—clearly much larger than any linearization bandwidths which might be achieved with the transmitter. Plots of Fig. 10 show that to achieve the highest degree of linearity, the open-loop bandwidth could be chosen to be anywhere in the range $0 < f_n < 2.5$ kHz as long as the $GBWD$ product is kept at its maximum allowable value.

III. Frequency-Hopped Transmitter

A general block diagram of the frequency-hopped transmitter is shown in Fig. 1. As with the basic fixed-carrier version, the baseband input signal is applied to the two arms of the transmitter in an I–Q format. A fraction of the RF output signal is applied to the input of the downconverter. Suitably scaled, the downconverted signal is then subtracted from the pure input signal. The error signal thus generated is filtered by first-order low-pass filters to remove its high frequency components, and the result is upconverted, preamplified, and finally applied to the RF amplifier.

If the total loop gain is sufficiently high and the feedback components do not add significant distortion, the result is a dramatic reduction in the distortion generated by the RF amplifier. As with the fixed-carrier transmitter, the level of reduction depends on a set of parameters such as loop gain, bandwidth and delay, nonlinear characteristics of the RF amplifier and imperfections of the loop feedback components.

A. Parameters Affected by Hopping

The parameters that can change in the hopping process are:

1) amplifier phase and gain (due to changes in frequency response);
2) amplifier AM–AM and AM–PM characteristics;
3) feedback gain/phase imbalance;
4) feedback dc offset.

1) Amplifier Frequency Response and Non-Linear Characteristics: If the change in the amplifier gain with frequency is negligible and its phase response is linear within the transmitter hopping bandwidth, the linearizing action of the transmitter at each carrier frequency will depend only on the amplifier AM–AM and AM–PM characteristics. If the amplifier nonlinear characteristics remain the same at the different operating frequencies, the transmitter performance will stay consistent, and similar degrees of linearization will be achieved throughout the hopping bandwidth.

Fig. 12 shows an example of the amplifier phase response, together with its linear approximation about carrier frequency ω_c. The linear approximation to the phase response is described by

$$\Phi(\omega) = \Psi(\omega_c) - (\omega - \omega_c)\tau \tag{7}$$

where $\Phi(\omega)$ is the linear approximation to the phase response, $\Psi(\omega_c)$ the phase at the carrier frequency, and τ the absolute value of the gradient of the straight line approximating the phase response. The latter is given by the amplifier group delay at the operating frequency defined by

$$\tau = \left| \frac{\partial}{\partial \omega} \Psi(\omega) \right|_{\omega_c}. \tag{8}$$

The baseband equivalent of (7), representing the variations of the amplifier phase response with the frequency of the components of the modulating signal (ω_b), is given by

$$\Phi(\omega_b) = \Psi(\omega_c) - \omega_b \tau. \tag{9}$$

Thus, the amplifier baseband equivalent phase response for each operating frequency may be approximated simply by inserting the appropriate value of $\Psi(\omega_c)$ into (9).

Equations (7) and (8) also show that the time delay generated by the amplifier remains constant if a straight line approximation can be used for its phase response within the hopping bandwidth. This is important since the linearization performance of the transmitter is determined by the level of

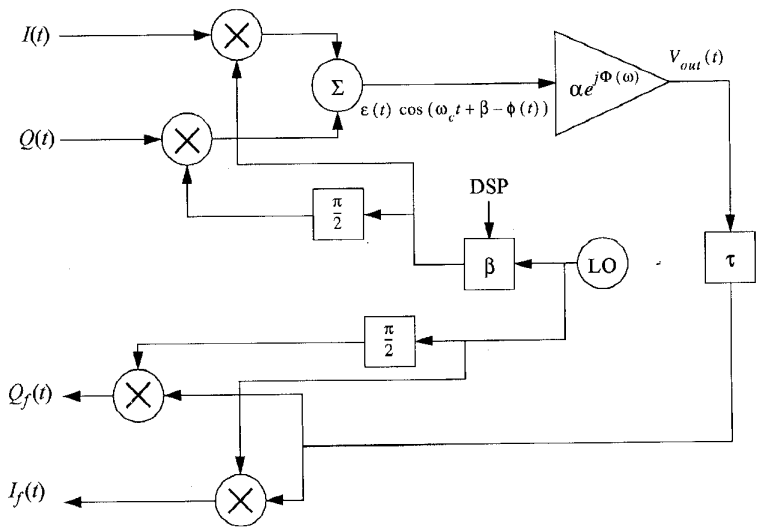

Fig. 13. Phasing the conversion stages using an RF phase-shifter.

its loop gain, and its stability by its gain-bandwidth-delay product as discussed before. Therefore, the value of loop time delay, determined mainly by the RF amplifier group delay, should remain relatively constant if consistent performance is to be achieved throughout the hopping process. Note that the frequency response of the loop baseband filters determines the loop order and its main frequency response characteristics. The group delay of these filters is hence incorporated in their phase response and should not be thought of as a source of excess loop delay. The loop delay discussed in this paper refers to the excess delay generated by other loop modules especially its RF components, e.g., RF preamplifiers and harmonic filter,[2] but mainly the power amplifier.

The stability of the feedback loop will be seriously affected by large[3] values of $\Psi(\omega_c)$. Hence it is necessary to compensate for this phase by appropriate phasing of the up- and down-conversion stages. As $\Psi(\omega_c)$ is dependent on the value of the carrier frequency, it is essential to somehow synchronize the conversion stages dynamically, i.e., by generating the correct phase compensation for each hopping frequency. In the case of a fixed-carrier transmitter, the phasing requirement may be achieved by placing a suitable length of coaxial cable between the local oscillator and the up-converter mixers. A voltage-controlled RF phase-shifter, which can be easily controlled by the DSP, may be used to generate the correct phasing for the frequency-hopped transmitter.

[2]A harmonic filter may be required at the output of the power amplifier in order to prevent translation of its harmonic zone components into baseband by the harmonics of the carrier generated by the down-converter mixers.

[3]The definition of "large" depends mainly on the nonlinear characteristics of the power amplifier and the required degree of transmitter linearity. In the case of the simulated 5-kHz transmitter, stability was maintained as long as $\Psi(\omega_c)$ fell within the range given by $-30^\circ < \Psi(\omega_c) < 30^\circ$. In general, the transmitter should be designed with large enough stability margins to accommodate possible variations in the frequency response of the power amplifier with temperature and aging. It should be noted however that for a highly linear transmitter where a high loop linear gain is applied, the changes in the linearity level with the variations in the amplifier frequency response can be negligible as long as the stability of the transmitter is maintained.

Fig. 13 shows the section of the transmitter including the amplifier, loop delay, conversion stages, and phase-shifter. The nonlinear nature of the amplifier is ignored for simplicity. The output of the amplifier is given by

$$V_{out}(t) = \alpha\varepsilon(t-\tau) \cdot \cos\{\omega_c t + [\Psi(\omega_c)+\beta] - \phi(t-\tau)\} \quad (10)$$

where α is the amplifier gain, β the phase generated by the phase-shifter, τ the amplifier group delay as before, and $(\varepsilon)(t)$ and $\phi(t)$ the envelope and phase of its input signal given by

$$\varepsilon(t) = \sqrt{I^2(t)+Q^2(t)}$$
$$\phi(t) = \tan^{-1}\frac{Q(t)}{I(t)}. \quad (11)$$

Consequently, the in-phase and quadrature components of the feedback signal can be obtained from (12). A close inspection of these components reveals the presence of an additional phase given by $[\Psi(\omega_c)+\beta]$, which adds to the transmitter loop phase, affecting its stability. However, as the value of β may be controlled by the DSP, it is possible to reduce the aforementioned phase to zero, and synchronize the conversion stages by applying the appropriate voltage to the phase-shifter

$$I_f(t) = \frac{\alpha\varepsilon(t-\tau)}{2}\cos\{[\phi(t-\tau)] - [\Psi(\omega_c)+\beta]\}$$
$$Q_f(t) = \frac{\alpha\varepsilon(t-\tau)}{2}\sin\{[\phi(t-\tau)] - [\Psi(\omega_c)+\beta]\}. \quad (12)$$

The spectral asymmetry caused by the amplifier AM–PM characteristics can also be reduced by further adjusting the phase-shifter generated phase. The value of this additional phase is determined by the amplifier nonlinear characteristics. Thus, the voltages corresponding to the values of phase required at each carrier frequency may be kept in a look-up table, which is then used by the DSP to control the phase-shifter in a suitable manner.

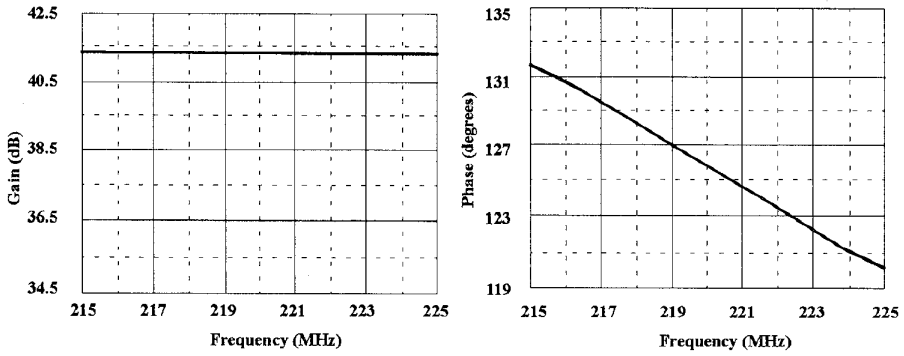

Fig. 14. Measured frequency response of the class AB amplifier used in the hardware prototype.

2) Feedback Gain/Phase Imbalance and dc Offset: The gain/phase imbalance and dc offset generated by imperfections in the feedback modules can degrade the transmitter performance severely [7]. However, the effects of these imperfections may be significantly reduced or even removed by predistorting the transmitter input signal. To eliminate the effects of feedback dc offset, the method described in [8] uses an envelope detector to measure the envelope level of the transmitter output signal while its input is set at zero. Feedback dc offset causes a nonzero output envelope level that can be reduced to zero by prebiasing the transmitter input signal. This is done by applying dc signals to the transmitter input and changing their level iteratively in a systematic manner until the output envelope is reduced to zero. The dc levels that result in the zero output envelope level are saved and added to the transmitter input signal in order to produce an output signal free of carrier feedthrough. In a similar fashion, the pre-distortion coefficients for the removal of feedback gain/phase imbalance are calculated by weighting known dc input signals until an expected output envelope is achieved. The final values of the weighting factors are saved as the predistortion coefficients.

The main sources of feedback gain/phase imbalance and dc offset are the imperfections of the down-converter mixers. Naturally, the change in the carrier frequency during the hopping process affects the levels of these imperfections which in turn necessitates the calculation of a different set of predistortion coefficients for each operating frequency. Fortunately, it is possible to generate these coefficients automatically as previously described. Once a full group of coefficients is evaluated, they can be stored in a look-up table, and applied by the DSP to the input signal as necessary. The contents of the look-up table may be updated periodically depending on the system timing allowances.

Although the gain/phase imbalance, mixer carrier feedthrough and dc offset in the transmitter forward path may cause some degradation in its output signal, in a highly linear transmitter where a large value of loop gain is applied, the effects of such imperfections are minimized by the feedback action. However, the transmitter automatic adjustment method mentioned above, can eliminate the problems resulting from the feedback gain/phase imbalance and dc offset and any residual degradations in the output signal caused by the forward path gain/phase imbalance and dc offset.

IV. Transmitter Prototype

To study the practicability of the Cartesian transmitter and its potential for frequency hopping purposes, a prototype operating at a centre frequency of 220 MHz with a hopping bandwidth of 10 MHz, and a linearization bandwidth of 5 kHz was constructed at the Centre for Communications Research, University of Bristol. As the main objective of the experiment was to examine the capability of the transmitter in a hopping environment, the focus was placed upon its hopping performance rather than optimizing its linearization capacity[4] (The latter has been achieved by other authors in the past [4]–[6]).

To avoid instability caused by the second system poles, relatively wideband (compared with the phase cross-over frequency of the first-order loop [11]) voltage-feedback[5] op-amps with a unity-gain bandwidth of 60 MHz were used (the bandwidth of the loop filters was about 2 kHz). Wideband RF components with bandwidths of a few tens of MHz were chosen to cover all possible carrier frequencies. The RF amplifier was a 300-mW-class AB amplifier whose frequency response and nonlinear characteristics at various carrier frequencies are shown in Figs. 14 and 15, respectively. The required control signals were generated by means of a DSP program.

A. Transmitter Transient Response

The speed at which a transmitter responds to switching conditions may be assessed by measuring its transient response. In the case of the Cartesian transmitter, two forms of transient response measurement need to be performed:

1) baseband transient response, which represents the transmitter speed of response to the switching conditions in its input signal;

[4]The prototype linearity could be improved significantly by a more careful design at the baseband layout stage. The long tracks connecting the baseband components in the present design have significant inductance values which together with the parasitic capacitances cause resonance at high frequencies (at about 2–3 MHz). As a result, the frequency response of the transmitter baseband section resembles that of a high-order system rather than the intended first-order system. Consequently, lower stability margins, lower permissible loop gain and worse linearity are resulted.

[5]The authors believe that the current-feedback op-amps whose closed-loop bandwidth is largely independent of their closed-loop gain can provide a better frequency response and hence better transmitter linearity.

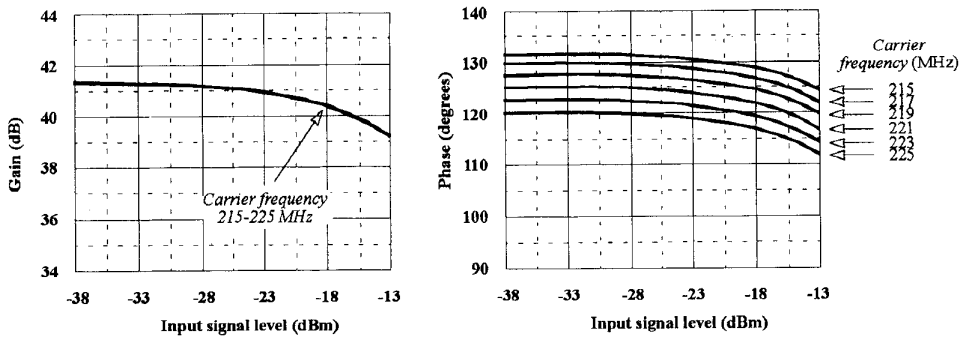

Fig. 15. Measured nonlinear characteristics of the class AB amplifier.

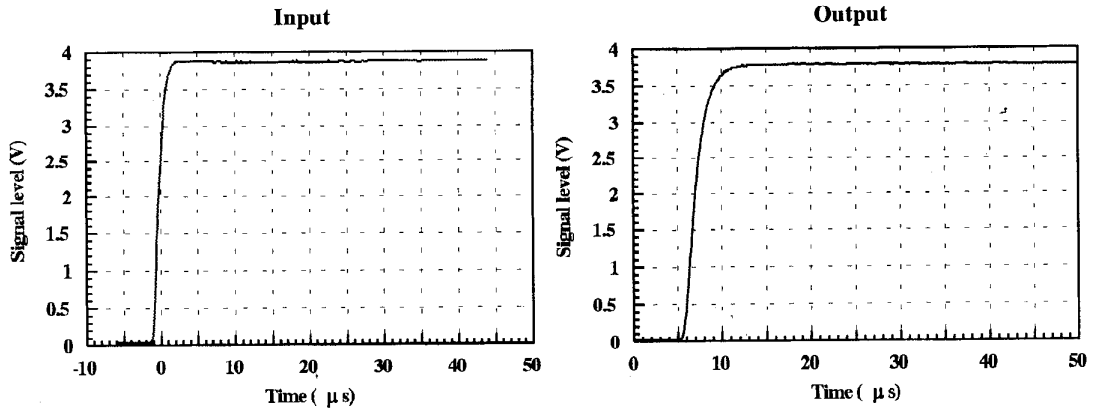

Fig. 16. Baseband transient response of the hardware prototype.

2) RF transient response, which is indicative of the transmitter speed of response to a switched carrier (i.e., a carrier that is switched off between consecutive hops).

In this section the nature of both forms of transient response is investigated and the results obtained from a hardware prototype are presented.

1) Baseband Transient Response: As discussed before, the baseband transient response of a Cartesian transmitter is determined by the size of its $GBWD$ product. Larger values of this parameter correspond to faster responses. Overshoots may be observed on the rising and/or falling edges of the output waveform when the $GBWD$ product is too large. The height of the overshoots may be reduced by lowering the $GBWD$ product at the expense of the transmitter linearization performance.

However, if the value of the $GBWD$ product is severely restricted by the feedback loop stability limits, the overshoots may never appear on the output waveform. This was the case in the hopping transmitter hardware prototype whose baseband transient response when excited by a complex square wave input signal is shown in Fig. 16.

To ensure a high degree of stability, the $GBWD$ product has been kept low. Despite the transmitter suboptimum linearizing performance, its baseband transient response is seen to be satisfactory: the output signal envelope takes about 6 μs to reach its maximum when the input signal envelope rises to its maximum in 4.2 μs.

2) RF Transient Response: Unfortunately, a good baseband transient response is not sufficient for the successful operation of a hopping transmitter which uses a switched carrier. The dc signal introduced in the feedback path by the down-converter mixers is amplified by the loop gain, generated by the modules situated between the down-converter and the transmitter output. In steady state conditions, the effect of the mixer generated dc offset may be removed by pre-biasing the transmitter input signal. However, if the local oscillator is turned on and off, as in the case of the switched carrier FH transmitter, the initial level of the dc offset can be large, and its effect severe when magnified by the loop action. The left hand plot of Fig. 17 shows the output signal when the transmitter input was reduced to zero, and the 220 MHz carrier was turned on and off. Although the carrier frequency was not changed in obtaining these results, the plot clearly demonstrates the transmitter RF transient response (the transmitter behavior would be similar if the carrier frequency were changed).

It is seen that the down-converter mixers react to the switched carrier by generating a train of impulses, which are amplified by the loop action. The up-converter mixers also contribute to this output, but as the loop gain applied to this contribution is much smaller than the gain applied to the down-converter contribution, the effect of the former may be assumed negligible. The presence of the overshoots can cause significant broadband interference, which is not acceptable, especially in a mobile environment.

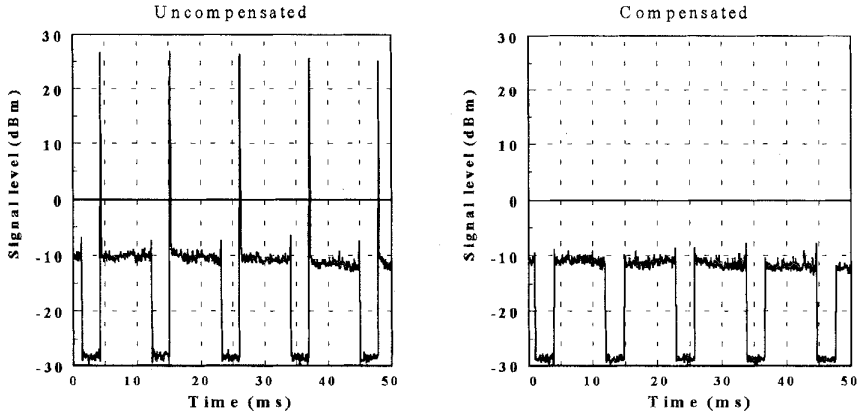

(a) (b)

Fig. 17. Hardware results: transmitter RF transient response (a) before and (b) after applying gain control. Analyzer settings: Atten.: 30 dB; RBW: 2.0 MHz; VBW: 100 kHz.

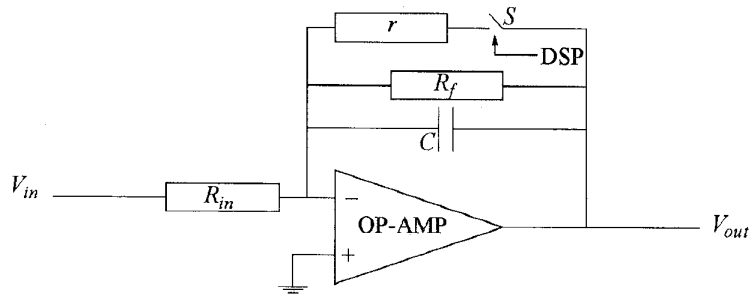

Fig. 18. Variable gain first-order filter.

The undesirable RF transient response can be totally avoided if a fast constant-envelope frequency synthesizer is available. To avoid possible instability caused by the local oscillator phase transients, and transmission of any unwanted RF signals, the loop gain must be reduced to zero between any two consecutive hops, thus the need for carefully designed control signals. The loop gain can be reduced at RF and/or baseband. However, if it is reduced by varying the RF amplifier gain, the unpredictable changes in the amplifier nonlinear characteristics during the process may result in the transmitter undergoing temporary instability. On the other hand, if the control over the loop gain is achieved at baseband, any unwanted signals generated in the process (e.g., spikes generated by CMOS switches) can be amplified by the loop action and appear at the transmitter output. In this paper, we concentrate on the performance of the switched-carrier transmitter, and consider the techniques which can be used to overcome its shortcomings.

B. Improving RF Transient Response

The transmitter RF transient response may be improved significantly by a number of methods, including local oscillator envelope shaping and reducing the feedback loop gain.

In the first method, the sharpness of the overshoots may be reduced by gradually ramping up the carrier signal instead of applying it to the mixers abruptly. This solution is not very flexible and, in practice, can be relatively difficult to implement.

A simpler technique for overcoming the problem of overshoots involves the reduction of the loop gain at the carrier signal switching instants. This can be done either at RF (i.e., reducing the RF amplifier and/or preamplifier gain) or baseband (i.e., reducing the gain of the loop baseband modules).

To improve the transient response of the transmitter prototype, the loop gain was reduced by changing the gain of its first-order filters. The block diagram of the first-order filter whose transfer function is given by (13) (R is the parallel equivalent of r and R_f) is shown in Fig. 18

$$\frac{V_{out}}{V_{in}} = \frac{-R}{R_{in}(1 + RC\omega j).} \tag{13}$$

By choosing r to be much smaller than R_f, the gain of the filters is reduced by a factor of $r/(r + R_f)$ when switch S (a CMOS switch) is closed. The filters' bandwidth, on the other hand, is increased by the same factor, keeping the loop $GBWD$ product constant. The large value of the filter bandwidth results in much shorter transients, which is another useful property of this technique.

The effectiveness of this technique when applied to the transmitter prototype is illustrated by the right-hand plot of Fig. 17. It can clearly be seen that the reduction in the loop baseband gain has decreased the height of the RF overshoots by about 35 dB, virtually removing the problem of RF transients. The control signal activating the switches

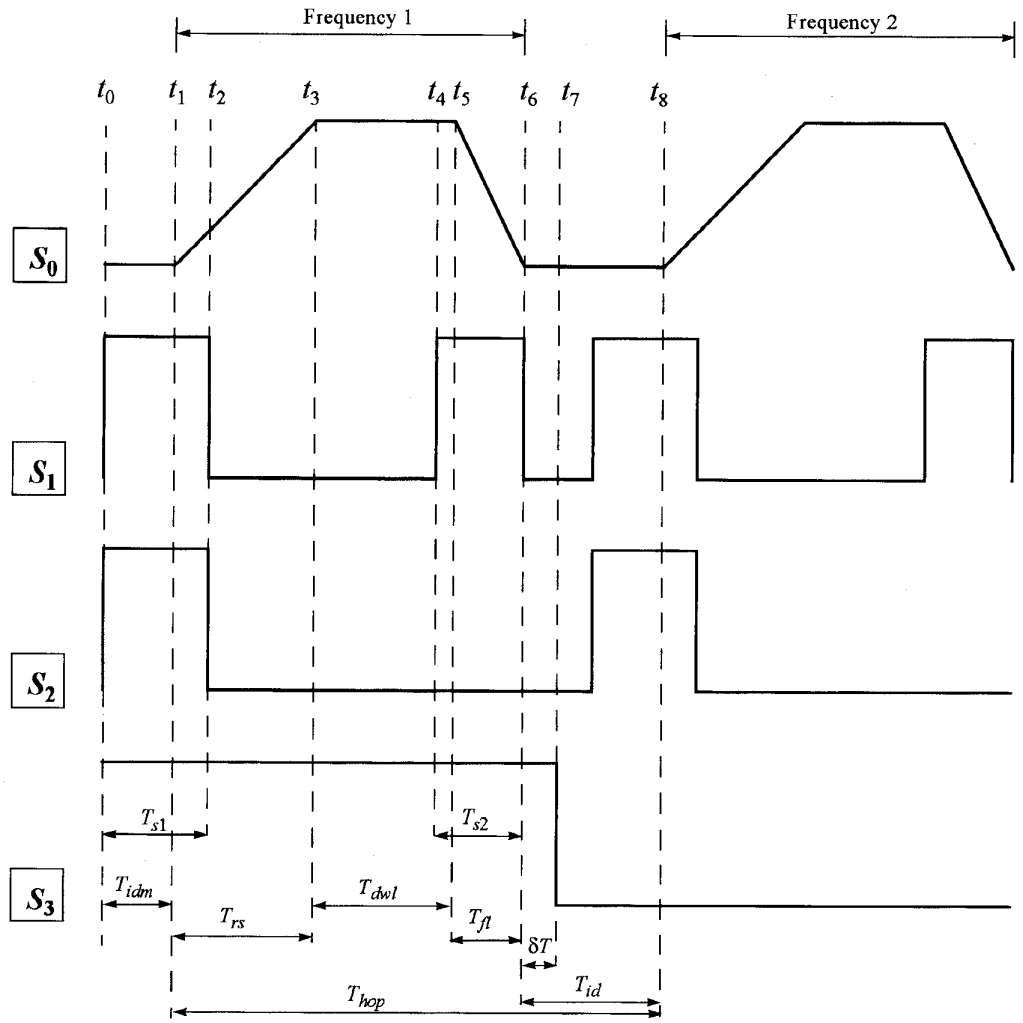

Legend

T_{idm}:Local oscillator signal minimum idle time
T_{dwl}:Local oscillator signal dwell time
T_{s1} :Trigger signal first on period
T_{rs} :Local oscillator envelope rise time
S_0 :Local oscillator envelope
S_1 :Frequency synthesizer and filter switch control signal (synthesizer in external trigger and dwell mode); logic 1 or 0
δT :Delay between the bottom of local oscillator envelope ramp-down and phase-shifter voltage transition instant
T_{id} :Total local oscillator signal idle time
T_{hop}:Hop period
T_{s2} :Trigger signal second on period
T_{fl} :Local oscillator envelope fall time
S_3 :Phase-shifter control signal; analogue
S_2 :Frequency synthesizer and filter switch control signal (synthesizer in external trigger, internal dwell mode); logic 1 or 0

Fig. 19. Transmitter DSP generated control signals and local oscillator envelope.

was provided by a DSP as discussed in the following section.

The relatively large steady-state output of the transmitter, shown in Fig. 17, may be reduced by a more careful removal of the feedback dc offset, e.g., by the technique described in [8] (in the case of the prototype under investigation, the feedback dc offset was measured manually, and compensated for using a look-up table).

C. Control Signals

The transmitter control signals need to be carefully generated for successful performance. Such signals may be produced

by means of a digital signal processor. The DSP can also be used to measure and remove the transmitter feedback imperfections which might otherwise severely degrade its performance. Some of the main functions of the DSP are:

1) triggering frequency synthesizer;
2) controlling loop gain;
3) generation of the phase-shifter control signal;
4) input signal predistortion;
5) baseband signal shaping.

The hopping carrier used with the transmitter prototype was generated by an HP 8645A Agile Signal Generator which could be operated in a number of modes. The two modes of interest, however, were "external trigger—internal dwell" and "external trigger—external dwell." In both modes, the carrier frequencies and the order in which they were applied were initially saved. The DSP was then used to generate a two-level signal (S_1 or S_2 in Fig. 19) which triggered the generator to turn on the carrier (external trigger). The time during which the carrier signal remained on was determined either externally (external dwell) by an additional trigger pulse (S_1), or internally (internal dwell) by saving the required dwell time and hop rate prior to starting the hop sequence. With this generator, the carrier envelope started to rise about 12 μs (T_{idm}) after the generator was triggered, imposing a minimum limit on the value of the carrier "idle time" (T_{id}), i.e., the time during which the carrier remained off between any two consecutive hops. The carrier switching time, i.e., the total of its rise and fall times ($T_{rs} + T_{fl}$), was about 3 μs.

The trigger signal, S_1 or S_2 in Fig. 19, was also employed to activate the CMOS switches whose function was discussed in Section IV-B. The undesirable overshoots resulting from the transmitter RF transient response appear as soon as the carrier signal is turned on, i.e., at instants such as t_1 and t_8. However, if the CMOS switches are already activated prior to the occurrence of the overshoots, the height of the overshoots may be reduced significantly. To ensure this effect, the duration of the first trigger pulse, T_{s1}, was chosen to extend just beyond the generator minimum idle time, T_{idm}.

A smaller overshoot occurs on the falling edges of the carrier signal at instants such as t_5. Closing the CMOS switches just before this instant can reduce its height. However, the spikes caused by the charge and/or discharge of the switches gate-channel capacitance at their opening or closing instants, e.g., t_4 and t_6, are amplified by the loop action, and if the carrier level is high when the spikes are generated, they will be relatively large (perhaps larger than RF transient overshoots) at the transmitter output. Thus it may be advantageous to activate the CMOS switches by a signal such as S_2, and tolerate the overshoots at the falling edges of the carrier signal. The right hand plot of Fig. 17 shows the transmitter RF transient response when the generator was operated in its external trigger—internal dwell mode, with a signal similar to S_2 activating both the generator and the switches.

To ensure transmitter stability, changes in the phase-shifter control voltage must occur while the loop gain is sufficiently low. The best time for changing this voltage is when the carrier signal is turned off, i.e., during the generator idle time (T_{id}).

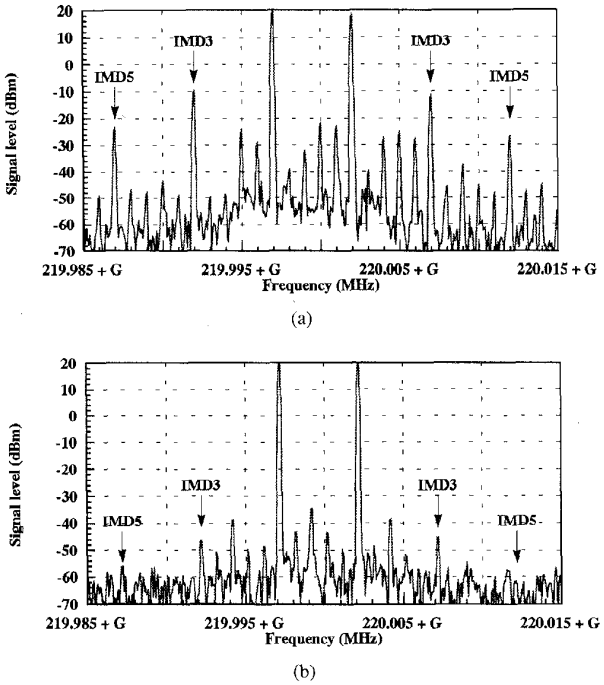

Fig. 20. Hardware results: FH transmitter open- and closed-loop output spectra $G = -5, \cdots, 0, \cdots, 5$. (a) Open loop. (b) Closed loop.

The appropriate values of control voltage can be stored in a look-up table and applied to the phase-shifter by the DSP when required.

D. Transmitter Output Spectrum

As the RF amplifier nonlinear characteristics remained unchanged[6] throughout the hopping bandwidth (Fig. 15), the transmitter level of linearity was expected to stay the same at all frequencies of interest. The measured two-tone test response of the hopping transmitter (Fig. 20) indicates the same level of linearity at various frequencies of operation, proving the validity of the theoretical prediction. In obtaining these results, the power amplifier was driven to its point of saturation.

The output spectrum of the hopping transmitter for carrier frequencies of 216, 217, 218, and 219 MHz is shown in Fig. 21, indicating no signs of instability. At the time of these measurements the hopping rate was set at 220 hops/s. It could, however, be increased to several hundred, depending on the parameters outlined in the previous section.

V. Calculation of Hopping Rate

As can be seen in Fig. 19, the total hopping period can be calculated from

$$T_{hop} = T_{dwl} + (T_{rs} + T_{fl} + T_{id}). \tag{14}$$

Assuming a negligible trigger pulse duration compared with $(T_{rs}+T_{fl}+T_{id})$, the hopping rate which will be mainly deter-

[6]Note that the vertical shift of the AM–PM characteristic along the phase axis is due to the amplifier phase response and can be compensated for by the function of the phase-shifter.

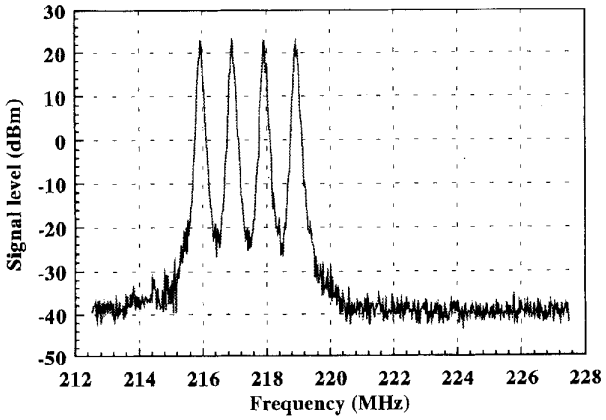

Fig. 21. Hardware results: transmitter hopping spectrum (hopping bandwidth of 4 MHz). Analyzer settings: Atten.: 30 dB; RBW: 100 kHz; VBW: 300 kHz; SWP: 48.3 s.

mined by the frequency synthesizer, transmitter linearization bandwidth, and in the case of digital transmission, number of symbols per hop and symbol pulse shape.

If the ratio of $(T_{rs} + T_{fl} + T_{id})$ to the total hopping period is given by n, then for a hopping rate of m hops per second the following relationship must be valid.

$$\frac{n}{m} = \overbrace{T_{rs} + T_{fl} + T_{id}}^{T_{sw}} \quad n < 1. \tag{15}$$

The relationship between T_{dwl} and the hop rate is given by

$$T_{dwl} = \frac{1-n}{m}. \tag{16}$$

When transmitting digital data, synthesizer dwell time T_{dwl}, symbol period (T_s), and number of symbols per hop (q) are related by (17), and the signal RF bandwidth (B_{RF}) is given by (18) (assuming a square pulse shape)

$$T_{dwl} = q \cdot T_s \tag{17}$$

$$B_{RF} \approx \frac{2}{T_s}. \tag{18}$$

Using (16)–(18), the following equation, expressing n in terms of q, B_{RF}, and T_{sw} is obtained

$$n = \frac{T_{sw} \cdot B_{\mathrm{RF}}}{2q + T_{sw} \cdot B_{RF}}. \tag{19}$$

The corresponding expression for the hopping rate is hence given by

$$m = \frac{B_{\mathrm{RF}}}{2q + T_{sw} \cdot B_{\mathrm{FR}}}. \tag{20}$$

In the case of a 5-kHz transmitter, with $T_{sw} = 15\ \mu$s (i.e., $T_{rs} + T_{fl} + T_{idm}$) and $q = 1$ symbol/hop, n and m are 3.6% and 2410 hops/s, respectively. Equation (20) shows that the hopping rate increases with an increase in B_{RF} and/or a decrease in q and/or T_{sw}.

As the RF bandwidth of the modulating signal is affected by the symbol pulse shape, the hopping rate is also a function of the pulse shape. If raised cosine filters are used to shape the symbols, the above relationships will be replaced by those given by

$$n = \frac{T_{sw} \cdot B_{\mathrm{RF}}}{(\alpha+1)(q+1) + T_{sw} \cdot B_{\mathrm{RF}}}$$

$$m = \frac{B_{\mathrm{RF}}}{(\alpha+1)(q+1) + T_{sw} \cdot B_{\mathrm{RF}}} \tag{21}$$

where α is the filter roll-off factor. Keeping T_{sw}, B_{RF}, and q as above, the corresponding values of n and m for $\alpha = 0.5$ are evaluated as 2.4% and 1626 hops/s, respectively.

VI. FH Transmitter Design Steps

The very first step in designing an FH Cartesian transmitter is choosing an amplifier which satisfies the power requirement and the conditions discussed in Section III-A. The amplifier must then be placed in the feedback loop with wideband RF components to test the transmitter linearization bandwidth and baseband transient response under fixed-carrier conditions. As discussed before, both of these are functions of the transmitter open-loop $GBWD$ product. When operating near the maximum value of $GBWD$ product, the baseband transient response may exhibit overshoots. Under such circumstances, depending on the settling time of the transient response, it may be necessary to reduce the value of the $GBWD$ product to achieve the required transient response. The improvement in the transient response is at the expense of a reduction in the level of transmitter linearity and consequently its linearization bandwidth. An excessive degradation in the linearization performance can be highly undesirable. Therefore, it is important to use an amplifier which can provide the satisfactory transient response and linearity level.

Choosing/designing a fast synthesizer, i.e., with a short enough switching time (T_{sw}), is the next necessary step. The maximum permissible value of the synthesizer switching time is found by inserting the maximum allowable value of n and the maximum required hopping rate in (15). This value can then be used to choose/design the suitable synthesizer for the FH transmitter.

After designing the frequency synthesizer and the fixed-carrier transmitter, the latter can be operated under frequency hopping conditions by applying the appropriate DSP control signals as discussed before.

The hopping speed, i.e., slow or fast, supported by the transmitter depends on the RF bandwidth of the signal to be transmitted, the nature of baseband signal pulses, the maximum tolerable value of n, i.e., $n_{\max}$, and the speed of the synthesizer. Using (21) and assuming $T_{sw} = 15\,\mu$s and $\alpha = 0.5$, the transmitter hopping rate and n are plotted against the signal RF bandwidth for various values of number of symbols per hop (q) in Fig. 22. Assuming $n_{\max} = 10\%$ and the transmitter linearization bandwidth is 25 kHz, plots of Fig. 22(b) indicate that for signal RF bandwidths of less than 22 kHz, the hopping transmitter can support slow, i.e., $q > 1$, as well as fast, i.e., $q < 1$, frequency hopping. When the signal RF bandwidth is larger than 22 kHz, the 25-kHz transmitter can only support slow frequency hopping. Fig. 22(a) shows that the maximum hopping rate corresponding to $n_{\max} = 10\%$, is about 6.7 kHz.

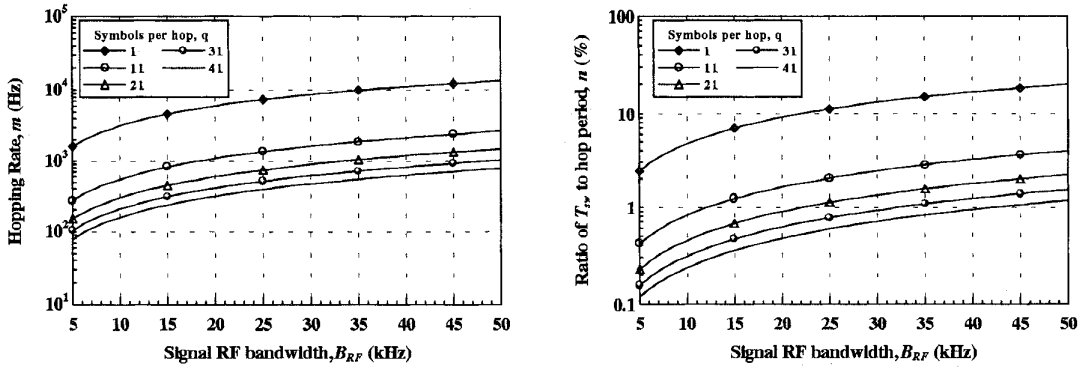

(a) (b)

Fig. 22. Plots of m and n versus signal RF bandwidth ($a = 0.5$, $T_{sw} = 15\,\mu$s).

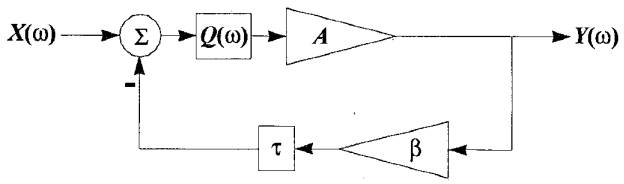

Fig. 23. First-order linear loop.

VII. Summary and Conclusions

In this paper, the frequency-hopped version of the Cartesian feedback linear transmitter has been examined. To investigate the effectiveness of the Cartesian feedback technique in removing the nonlinearities of the RF amplifiers under hopping conditions, a hardware prototype with wideband RF components was constructed at Bristol. The results from this model indicate that as long as the amplifier gain response remains unchanged, its phase response is linear within the hopping bandwidth, its nonlinear characteristics do not vary significantly with the change in the carrier frequency and the baseband transient response of the fixed-carrier transmitter is satisfactory, it is perfectly possible to maintain the high level of linearity generated by the basic transmitter throughout a wide hopping bandwidth. In other words, once the above conditions are met, the transmitter stability and linearization performance will remain the same at all hopping frequencies without the need to change any of the loop parameters, i.e., gain and bandwidth, during the hopping process. However, changes in the amplifier phase response and feedback imperfections with frequency may need to be adaptively compensated for if affecting the transmitter stability and linearization performance.

The transmitter baseband transient response, governed by the size of its $GBWD$ product, is mainly determined by the characteristics of the RF amplifier (i.e., its nonlinear characteristics and group delay). Its RF transient response, on the other hand, depends on the size of the loop gain generated by the components situated between the down-converter mixers and the transmitter output, and the shape of the carrier envelope applied to the down-converter mixers. Hence, the RF transient response can be significantly improved by shaping the latter and/or reducing the loop gain at the carrier switching instants. In the case of the transmitter hardware prototype, this was achieved at baseband by changing the gain of loop filters.

The results obtained from the prototype suggest that the Cartesian feedback technique can be successfully used under frequency hopping conditions, as long as a hopping carrier with fast switching times is available. The frequency-hopped Cartesian transmitter provides the possibility of using spectrally efficient linear modulation techniques with frequency hopping for use in third generation communication systems. Amongst the advantages of such a transmitter are:

1) efficient use of the valuable frequency spectrum;
2) much lower values of adjacent and co-channel interference;
3) smaller, lighter, and more power-efficient transmitter;
4) larger system capacity;

which are all of extreme value, considering the ever-increasing demand for mobile communications.

Appendix A
Stability Margins of First-Order Linear Loops

The open loop frequency response of a first-order linear loop with time delay (Fig. 23) is given by (22), where ω and ω_n are frequency and the loop 3-dB bandwidth in rads/s, with τ and G representing the loop delay and gain, respectively. G in this equation includes both feedback and forward gains, i.e., $G = A\beta$, and τ represents the sum of all delays around the loop. The filter frequency response, $Q(\omega)$, is given by

$$H(\omega) = \frac{G\omega_n}{\omega_n + j\omega} e^{-j\omega\tau} \tag{22}$$

$$Q(\omega) = \frac{\omega_n}{\omega_n + j\omega}. \tag{23}$$

Fig. 24 shows the open-loop frequency response of the first-order system plotted on the complex plane. Point A in this figure corresponds to the loop gain crossover frequency ω_{ge}, i.e., the frequency at which the open-loop gain is unity. ω_{pc}, the frequency at which the loop phase becomes π rads, is known as the phase crossover frequency, corresponding to point B in Fig. 24

$$GM = \frac{1}{|H(\omega_{pc})|} \tag{24a}$$

$$PM = \angle H(\omega_{gc}) + \pi \tag{24b}$$

$$|H(\omega)| = \frac{G\omega_n}{\sqrt{\omega^2 + \omega_n^2}} \tag{25a}$$

$$\angle H(\omega) = -\left[\tan^{-1}\left(\frac{\omega}{\omega_n}\right) + \omega\tau\right]. \tag{25b}$$

The loop gain and phase margins (denoted by GM and PM, respectively) can be found from (24). Using (22), the loop gain and phase responses are evaluated as in (25a) and (25b). The phase cross-over frequency is then found by setting the loop phase at π rads. Simplification of the resulting equation yields

$$\tan \omega\tau = -\frac{\omega}{\omega_n}. \tag{26}$$

Due to the periodic nature of $\tan \omega\tau$, there are infinite number of solutions to the above equation. However, the graphical consideration of (26) (see Fig. 25) reveals that the first crossover frequency (corresponding to point A in Fig. 25) occurs when

$$\frac{\pi}{2\tau} < \omega < \frac{2\pi}{2\tau}. \tag{27}$$

Hence, using the Taylor series expansion of $\tan \omega\tau$ about $\pi/2$ (28), the solution to (26) may be written as in (29), which is reduced to (30) for small $\omega_n\tau$. It should be noted that the Taylor expansion used in this analysis closely approximates $\tan \omega\tau$ virtually throughout the range defined by (27)

$$\tan \omega\tau \approx \frac{-2}{2\omega\tau - \pi} + \frac{2\omega\tau - \pi}{6} \tag{28}$$

$$\omega_{pc} \approx \frac{3\pi + 2\pi\omega_n\tau + \sqrt{9\pi^2 + 144\omega_n\tau + 48\omega_n^2\tau^2}}{12\tau + 4\omega_n\tau^2} \tag{29}$$

$$\omega_{pc} \approx \frac{\pi}{2\tau}. \tag{30}$$

The loop gain at the phase cross-over frequency is then found by substituting (30) in (25a), giving

$$|H(\omega_{pc})| \approx \frac{G\omega_n}{\sqrt{\frac{\pi^2}{4\tau^2} + \omega_n^2}} \approx \frac{2G\omega_n\tau}{\pi} \quad \text{For } \omega_n\tau \ll \frac{\pi}{2} \tag{31}$$

resulting in a gain margin of

$$GM \approx \frac{\pi}{2G\omega_n\tau}. \tag{32}$$

As the gain margin of a stable loop is larger than unity, the upper limit of loop gain is found as

$$G_{\max} \approx \frac{\pi}{2\omega_n\tau}. \tag{33}$$

To evaluate the phase margin, the gain crossover frequency must be found by setting the left-hand side of (25a) at unity and solving the resulting equation:

$$\omega_{gc} = \omega_n\sqrt{G^2 - 1} \approx \omega_n G \quad \text{For } G \gg 1. \tag{34}$$

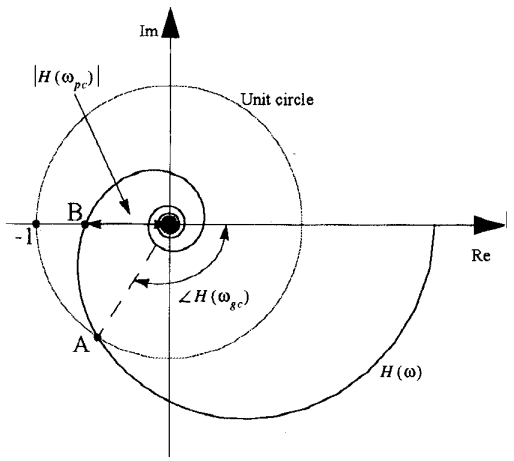

Fig. 24. Open-loop Nyquist plot of a first-order loop including delay.

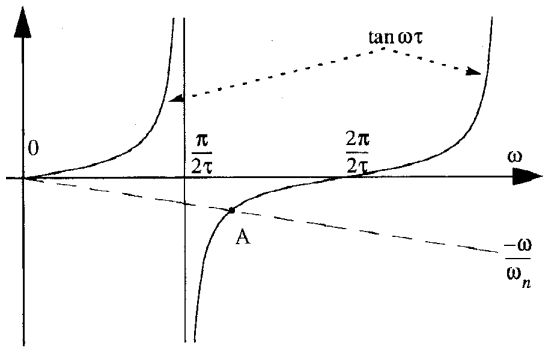

Fig. 25. Plots $\tan \omega\tau$ of and $-\omega/\omega_n$ versus frequency.

The loop phase at this frequency is then found as

$$\angle H(\omega_{gc}) = -\left(\tan^{-1}\sqrt{G^2 - 1} + \omega_n\tau\sqrt{G^2 - 1}\right) \approx -\left(\frac{\pi}{2} + G\omega_n\tau\right) \quad \text{For } G \gg 1. \tag{35}$$

The phase margin is consequently found by substituting (35) in (24b)

$$PM \approx \frac{\pi}{2} - G\omega_n\tau. \tag{36}$$

The phase margin of a stable loop must be positive, hence

$$G < \frac{\pi}{2\omega_n\tau}. \tag{37}$$

Comparison of (33) and (37) shows that the loop stability is guaranteed if its gain-bandwidth-delay product satisfies

$$G\omega_n\tau < \frac{\pi}{2}. \tag{38}$$

APPENDIX B
VARIATIONS OF DISTURBANCE ATTENUATION WITH LOOP GAIN AND BANDWIDTH

The portion of the output of a linear feedback system (Fig. 26) affected by a forward path disturbance, D, is given

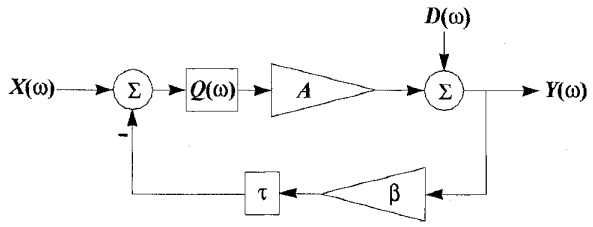

Fig. 26. Linear loop with forward path disturbance.

by

$$Y_D(\omega) = \frac{D(\omega)}{1 + A\beta Q(\omega)e^{-j\omega\tau}}. \tag{39}$$

When the loop gain at a given frequency is much larger than unity, the effect of the loop phase may be ignored. Consequently, the disturbance attenuation, i.e., the magnitude of the denominator of the right hand side of (39), will be determined by the filter magnitude response and loop gain. In the case of a first-order system, the former is a function of the filter 3-dB bandwidth (24a). Therefore, the attenuation level may be controlled by varying loop gain and/or 3-dB bandwidth.

In the case of a first-order loop, the distortion attenuation factor at relatively low frequencies (i.e., $\omega \ll A\beta\omega_n$), where loop gain is much larger than unity, may be approximated by

$$ATT \approx \frac{A\beta\omega_n}{\sqrt{\omega_n^2 + \omega^2}}. \tag{40}$$

The attenuation level is maximized by maximizing the gain-bandwidth product, $A\beta\omega_n$, and minimizing the filter 3-dB bandwidth, ω_n. For a given time delay the maximum value of gain-bandwidth product is determined from (38).

Plots of Fig. 27 show the effect of the variations in the loop 3-dB bandwidth on the disturbance attenuation with the GBW (Gain-Bandwidth) product at its maximum. It can be seen that a reduction in the loop bandwidth, and consequently an increase in its gain, results in a weaker disturbance at the output. This property of the loop can also be seen by substituting the GBW product by a constant K and rewriting (40) as

$$ATT \approx \frac{K}{\sqrt{\left(\frac{K}{A\beta}\right)^2 + \omega^2}}. \tag{41}$$

Equation (41) shows that for a given disturbance frequency, the attenuation level increases asymptotically with loop gain. It also indicates that the changes in the attenuation level with loop gain are much larger for $A\beta \ll K/\omega$ than for $A\beta \gg K/\omega$. Maximum attenuation level is achieved when the loop gain approaches infinity (loop bandwidth approaches zero). The value of this maximum is frequency-dependent and is given by (42). The plots of Fig. 28 illustrate the effect of variations in the loop gain on the disturbance attenuation level for various disturbance frequencies

$$ATT \approx \frac{K}{\omega}. \tag{42}$$

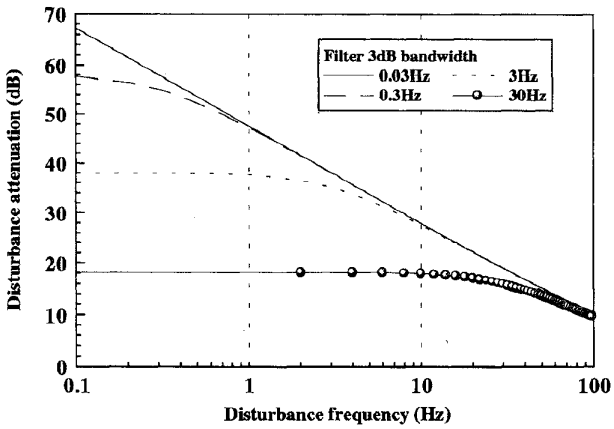

Fig. 27. Effect of loop 3-dB bandwidth on disturbance attenuation level (fixed GBW product).

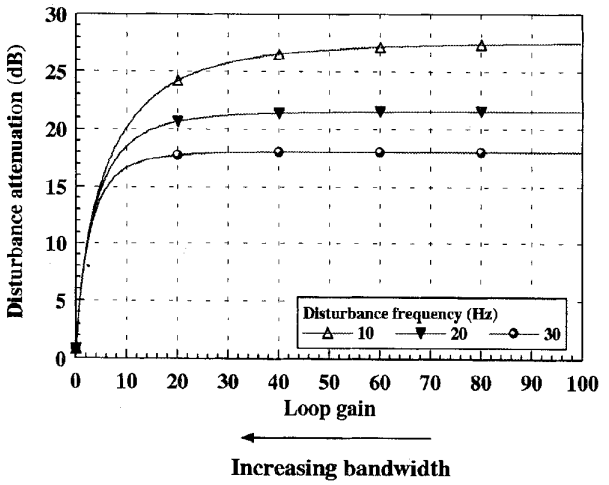

Fig. 28. Effect of loop gain on disturbance attenuation level for a fixed $GBWD$ product (delay = 1 ms, $GBWD = 0.24$).

Appendix C
Closed-Loop 3-dB Bandwidth of First-Order Linear Loops

The frequency response of the first-order loop of Fig. 23 is given by (43). Approximating $e^{-j\omega\tau}$ by its first-order Taylor series about $\omega\tau = 0$, this equation may be rewritten as in (44)

$$Y(\omega) = \frac{A\omega_n}{j\omega + \omega_n + A\beta\omega_n e^{-j\omega\tau}} \cdot X(\omega) \tag{43}$$

$$Y(\omega) = \frac{A\omega_n}{j\omega + \omega_n + A\beta\omega_n(1 - j\omega\tau)} \cdot X(\omega). \tag{44}$$

A good approximation to the closed-loop 3-dB bandwidth can then be found by finding the frequency at which the real and imaginary parts of the denominator of the RHS of (44) are equal (45). For an ideal case, where $\tau = 0$, the closed-loop 3-dB bandwidth is given by (46). Equations (45) and (46) show that when the open-loop gain, i.e., $A\beta$, is larger than unity, which is the case in most practical situations, the closed-loop 3-dB bandwidth is larger than the open-loop 3-dB bandwidth given by ω_n. These equations also indicate that for fixed values

of delay and $GBWD$ product, the variations in open-loop gain and bandwidth (as discussed in Appendix II) do not affect the closed-loop 3-dB bandwidth as long as $A\beta \gg 1$.

$$BW_{cl\,3\,\mathrm{dB}} \approx \frac{(1+A\beta)\omega_n}{1-A\beta\omega_n\tau} \tag{45}$$

$$BW_{cl\,3\,\mathrm{dB}} = (1+A\beta).\omega_n \tag{46}$$

Appendix D
Loop Transient Response

The transient response of a linear control loop is determined by the level of its relative stability. A system which has large stability margins exhibits better transient response than one whose stability can be disturbed by small variations of loop gain and/or phase [9].

The unit step response of a system is usually used to measure its transient behavior. The unit step response of an ideal first-order loop (without delay) is given by (47). Equation (48) gives the loop settling time, defined as the time taken for the output signal to reach $\alpha\%$ of its final value. For a given value of α, the settling time is reduced with an increase in the loop gain-bandwidth product

$$y(t) = \frac{A}{1+A\beta}\left[1 - e^{-(1+A\beta)\omega_n t}\right] \tag{47}$$

$$t_s = \frac{\ln\left(\dfrac{100}{100-\alpha}\right)}{(1+A\beta)\omega_n}. \tag{48}$$

As indicated by (47), the transient response of an ideal first-order system is always exponential. However, when the time delay is taken into account, the nature of the transient response will become dependent on the size of the $GBWD$ product. Consider the Laplace transform of the unit step response of the first-order loop with delay as given by

$$Y(s) = \frac{1}{s} \cdot \frac{A\omega_n}{\omega_n + s + A\beta\omega_n e^{-s\tau}}. \tag{49}$$

Assuming a small value of time delay and approximating $e^{-s\tau}$ by its second-order Taylor series (50), (49) may be rewritten as

$$e^{-s\tau} \approx 1 - \tau s + \tfrac{1}{2}\tau^2 s^2 \tag{50}$$

$$Y(s) = \frac{A\omega_n}{s[0.5A\beta\omega_n\tau^2 s^2 + (1-A\beta\omega_n\tau)s + (1+A\beta)\omega_n]}. \tag{51}$$

Depending on the value of the $GBWD$ product and assuming $\omega_n\tau \ll 1$, three different cases of transient response may be considered [10].

1) Critically Damped: When the $GBWD$ product satisfies (52), the transient response of the loop will be exponential and its settling time at a minimum. This response is described as critically damped

$$A\beta\omega_n\tau \approx \frac{1}{1+\sqrt{2}}. \tag{52}$$

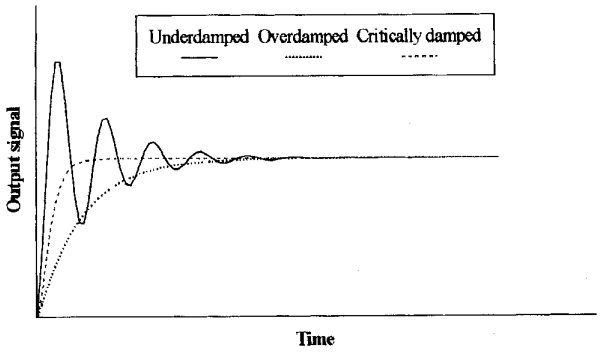

Fig. 29. The three types of transient response.

2) Overdamped: When the value of $GBWD$ product falls in the region outlined by (53), the transient response maintains its exponential nature but longer settling times than the case of critical damping will result. This response is described as overdamped

$$0 < A\beta\omega_n\tau < \frac{1}{1+\sqrt{2}}. \tag{53}$$

3) Underdamped: When the condition given in (54) is met, The pure exponential nature of the response is lost and it exhibits overshoots. The transient response in this case is described as underdamped

$$A\beta\omega_n\tau > \frac{1}{1+\sqrt{2}}. \tag{54}$$

Note that to maintain steady state stability the upper limit of the $GBWD$ product must not exceed the value given by (38). The three cases of transient response described above are compared in Fig. 29, demonstrating the dependence of the transient response on $GBWD$ product. The choice of $GBWD$ product depends on the trade-off between the acceptable output disturbance level and the loop transient response.

Acknowledgment

The authors would like to thank the Centre for Communications Research (CCR), University of Bristol for the provision of laboratory facilities, and members of the CCR for their assistance throughout this work.

References

[1] D. J. Purle, S. C. Swales, M. A. Beach, and J. P. McGeehan, "Frequency hopped CDMA for third generation mobile radio systems," in *43rd IEEE Veh. Tech. Conf.*, Secaucus, NJ, May 1993, vol. 18, no. 20, pp. 692–695.

[2] A. R. Nix, R. J. Castle, and J. P. McGeehan, "The application of 16 APSK to mobile fading channels," in *Proc. IEE 6th Int. Conf. Mobile Radio and Personal Comm.*, Warwick, U.K., Dec. 1991, pp. 231–236.

[3] S. Chennakeshu and G. J. Saulnier, "Differential detection of $\pi/4$-shifted-DQPSK for digital cellular radio," *IEEE Trans. Veh. Technol.*, vol. 42, pp. 46–57, Feb. 1993.

[4] R. J. Wilkinson, J. Macleod, M. A. Beach, and A. Bateman, "Linear transmitter design for MSAT terminals," in *2nd Int. Mobile Satellite Conf.*, Ottawa, Ont., Canada, June 1990, pp. 297–301.

[5] A. Bateman, D. Haines, and R. Wilkinson, "Direct conversion linear transmitter design," in *IEEE Int. Conf. Mobile and Personal Comm.*, Warwick, U.K., Dec. 1989.

[6] V. Petrovic, "Reduction of spurious emission from radio transmitters by means of modulation feedback," in *IEE Conf. Radio Spectrum Conservation Tech.*, Sept. 1983, pp. 44–49.

[7] M. Boloorian, J. P. McGeehan, and R. J. Wilkinson, "Dynamic performance evaluation of the Cartesian feedback linear transmitter," *IEE Colloq. on Linear Amplifiers and Transmitters,* Apr. 1994, vol. dig. 1994/089.
[8] M. Boloorian and J. P. McGeehan, "Automatic adjustment of the Cartesian feedback linear transmitter," submitted to *IEEE Proc.-Communications,* May 1994.
[9] B. C. Kuo, *Automatic Control Systems,* 3rd ed. Englewood Cliffs, NJ: Prentice-Hall, 1975, p. 475.
[10] S. M. Shinners, *Modern Control System Theory and Application,* 2nd ed. Reading, MA: Addison-Wesley, 1978, ch. 4.
[11] M. Boloorian and J. P. McGeehan, Maximisation of Cartesian transmitter linearlisation bandwidth," *IEE Electron. Lett.*, vol. 32, no. 19, pp. 1823–1824, Sept. 1996.

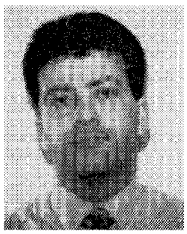

Majid Boloorian (M'95–A'96) received the B.Eng. (Hons.) degree in electrical and electronic engineering from the University of Manchester, Institute of Science and Technology (UMIST), Manchester, U.K., in 1990, and the Ph.D. degree in communications engineering from the University of Bristol, U.K., in 1995.

Since 1994, he has been a Research Associate at the Centre for Communications Research, University of Bristol. During 1990–1991, he was a Research Assistant at the University of Cambridge, U.K. His research interests include RF amplifier linearization techniques, digital communications, and digital signal processing.

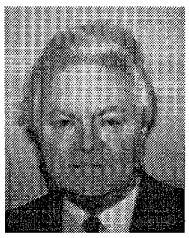

Joseph P. McGeehan received the B.Eng. and Ph.D. degrees in electrical and electronic engineering from the University of Liverpool, U.K., in 1967 and 1971, respectively.

In 1970, he was appointed Senior Scientist at the Allan Clark Research Centre, Plessey Company Ltd., where he was responsible for the research and development of two- and three-terminal Gunn Effect Devices and their application to high-speed logic, telecommunications, and radar systems. In 1972, he became an Academic Staff Member of the School of Electrical Engineering of the University of Bath, U.K., and initiated research in SSB (subsequently linear modulation) for mobile radio. In 1984, he was appointed to the Chair of Communications Engineering at the University of Bristol. He is presently Head of Department of Electrical and Electrical Engineering and Director of the University Research Centre in Communications Engineering.

Dr. McGeehan received the IEE Proceedings Mountbatten Premium award and the IEEE Transactions Neal Shephard Award and awards from Motorola Research Foundation (U.S.) and Schlumberger Industries (France) for his research contributions to radio communications. He serves on numerous national and international committees concerned with mobile communications. He is a Fellow of the IEE, the Royal Academy of Engineering, and the Royal Society of Arts and Commerce.